Chapter 10

Feedback Loops in Biological Networks

Elisa Franco and Kate E. Galloway

Abstract

We introduce fundamental concepts for the design of dynamics and feedback in molecular networks modeled with ordinary differential equations. We use several examples, focusing in particular on the mitogen-activated protein kinase (MAPK) pathway, to illustrate the concept that feedback loops are fundamental in determining the overall dynamic behavior of a system. Often, these loops have a structural function and unequivocally define the system behavior. We conclude with numerical simulations highlighting the potential for bistability and oscillations of the MAPK pathway re-engineered through synthetic promoters and RNA transducers to include positive and negative feedback loops.

Key words Feedback, Bistability, Oscillations, MAPK pathway, Synthetic biology

1 Introduction

Cells sense their environment and make decisions through coordinated molecular events. The dynamic interactions among nucleic acids, enzymes, and small molecules define such molecular events and specify their possible outcomes. For example, a set of reactions among a set of enzymes and genes may trigger transient, sustained, or periodic responses in other enzymes, depending on external stimuli [1]. Feedback among molecular components plays a crucial role in defining such complex behaviors, and synthetic feedback loops are routinely designed to redirect cellular responses and fate [2].

Mathematical models capturing the behavior of a molecular system are useful to support and guide experiments [3]. Feedback loops may result in counterintuitive behaviors in a system, thus a combination of numerical and theoretical analysis of a validated model can yield important insights, for example helping to identify the key species and parameters. Models can often be simplified to focus on such key reactions, and it may be possible to achieve valid conclusions on the behavior of the system without having to resort to extensive numerical simulations [4].

Mario Andrea Marchisio (ed.), *Computational Methods in Synthetic Biology*, Methods in Molecular Biology, vol. 1244,
DOI 10.1007/978-1-4939-1878-2_10,

In this chapter, we focus on classical methods from dynamical systems and control theory that can be used on ordinary differential equation (ODE) models of molecular networks. We begin by briefly introducing ODE models through the mitogen-activated protein kinase (MAPK) pathway, for which a hierarchy of models of different complexity is available in the literature [4–6]. ODE models for molecular networks always include nonlinear terms: we introduce the concept of linearization, through which one can systematically explore the behavior of a system in a neighborhood of its stationary points. We illustrate this simple method with several examples, in particular the MAPK pathway.

In Subheading 4.1 we highlight the concept that feedback loops can unequivocally determine the possible dynamic responses of a system. Some of the first and best known mathematical conjectures in this area were formulated by R. Thomas [7], and focus on the presence of positive or negative feedback loops in the linearized model of a system (loops in the Jacobian graph): a negative feedback loop is a necessary condition for stable periodic behavior, while a positive loop is a necessary condition for multistationarity (*see* [8] for a very thorough survey). These conjectures were proved in [9] and [10], with several further extensions and refinements [11–14]. While Thomas' conjectures are only necessary, they have been helpful in guiding the design of numerous synthetic molecular circuits [15–24]. We conclude with numerical simulations exploring the potential for bistability and oscillations of the MAPK pathway in yeast, re-engineered to include artificial positive and negative feedback through synthetic promoters and RNA gates [25].

2 Dynamic Models for Molecular Systems

Deterministic ODEs are commonly adopted in conventional engineering fields: ODEs are easily derived directly from the laws of physics, thermodynamics, and electromagnetism, and are a good description of macroscopic systems where stochastic effects are negligible. Molecular systems operating at high copy numbers have been successfully modeled using ODEs; for gene networks, alternative descriptions include stochastic equations or boolean models [3]. The MAPK pathway is a well-known signal transduction network which has been successfully modeled using ODEs: we will use it as our example system throughout this chapter.

One can identify two main approaches to the derivation of ODE models for biochemical systems. The first is a mechanistic approach, whereby the modeler tries to identify all possible chemical reactions that contribute to the process behavior; this approach is particularly fruitful in well-characterized systems (for example, understood model pathways or in vitro networks), but the resulting

models may be extremely complex and require heavy numerical treatment. The famous Huang–Ferrell model of the MAPK pathway [5] is one of the best examples of this approach. A list of ten reactions is used to model the three-stage, double phosphorylation pathway, and build 18 ODEs with 30 parameters using the mass action kinetics formalism. To illustrate this process, we consider solely the activation stage of the cascade, where MAPKKK, which we denote as m_{3K} for brevity, is activated (m^*_{3K}) and inactivated, respectively, by two "input" enzymes u_1 and u_2. These reactions are:

$$m_{3K} + u_1 \underset{r_1}{\overset{f_1}{\rightleftharpoons}} m_{3K} \cdot u_1 \xrightarrow{k_1} m^*_{3K} + u_1,$$
$$m^*_{3K} + u_2 \underset{r_2}{\overset{f_2}{\rightleftharpoons}} m^*_{3K} \cdot u_2 \xrightarrow{k_2} m_{3K} + u_2.$$

The corresponding ODEs associated with these isolated reactions for M_{3K} activation/inactivation are:

$$\frac{d\, m_{3K}}{dt} = -f_1\, m_{3K}\, u_1 + r_1\, m_{3K} \cdot u_1 + k_2\, m^*_{3K} \cdot u_2,$$
$$\frac{d\, m_{3K} \cdot u_1}{dt} = +f_1\, m_{3K}\, u_1 - (r_1 + k_1) m_{3K} \cdot u_1,$$
$$\frac{d\, m^*_{3K}}{dt} = -f_2\, m^*_{3K}\, u_2 + r_2\, m^*_{3K} \cdot u_2 + k_1\, m_{3K} \cdot u_1,$$
$$\frac{d\, m^*_{3K} \cdot u_2}{dt} = +f_2\, m^*_{3K}\, u_1 - (r_2 + k_2) m^*_{3K} \cdot u_1.$$

However, when considered in the context of the entire pathway, M^*_{3K} binds and phosphorylates M_{2K}: thus, the ODEs describing the dynamics of M^*_{3K} include additional second order terms. This example highlights the rapidly growing size and complexity of detailed models built using mass action kinetics. Nevertheless, it must be noted that the mass action formalism allows to derive ODEs systematically once reactions are specified, and many free software tools are available to automatically perform this operation [26, 27].

The second approach is phenomenological and driven by sensible approximations that describe qualitatively the observed dynamics; this approach generally yields models more amenable to analytical treatment, which however may not capture faithfully the system's dynamics and ignore several sources of uncertainty. Using a combination of mathematical analysis and numerical simulations supported by experimental data, the Huang–Ferrell model can be collapsed into a simpler, gray-box model where several intermediate reactions are captured by cooperative Hill functions. For instance, the dynamics of a kinase species x being doubly phosphorylated by its input u (where the input is

the upstream kinase), yielding active kinases x_p and $x_{p\ p}$, can be written as [28]:

$$\frac{dx}{dt} = -uk_1 \frac{x}{K_1 + x} + V_2 \frac{x_p}{K_2 + x_p},$$
$$\frac{dx_p}{dt} = uk_1 \frac{x}{K_1 + x} - V_2 \frac{x_p}{K_2 + x_p} - uk_3 \frac{x_p}{K_3 + x_p} + V_4 \frac{x_{pp}}{K_4 + x_{pp}},$$
$$\frac{dx_{pp}}{dt} = uk_3 \frac{x_p}{K_3 + x_p} - V_4 \frac{x_{pp}}{K_4 + x_{pp}},$$

where V_i are the maximal enzyme rates, k_i are the catalytic rate constants, and K_i are the Michaelis constants [28]. The readers familiar with Michaelis–Menten enzyme kinetics will immediately recognize that the functional terms in the equations above come from a simple assumption of timescale separation between the binding/unbinding dynamics of an enzyme to its substrate, and the catalytic step of the reaction. By solving numerically the equations above for plausible reaction parameters we find that, as a function of a constant input concentration u, the doubly phosphorylated kinase x_{pp} at the end of the cascade exhibits a switch-like response. If matching steady-state behavior is the objective of the model, one could further collapse the equations above into a first order system that relates the input u with the output of the cascade $m = x_{pp}$:

$$\frac{dm}{dt} = \frac{\alpha u^n}{K_M^n + u^n} - m,$$

where now m indicates the concentration of doubly phosphorylated kinase, and parameters α, K, and n are chosen to capture to the observed input/output relationship.

Based on this simplified model for the double phosphorylation process of each kinase, one can assemble a naive phenomenological model for the entire cascade:

$$\begin{aligned}
\frac{dm_3}{dt} &= \alpha_3 \frac{u^{n_3}}{K_{M3}^{n_3} + u^{n_3}} - m_3 \\
\frac{dm_2}{dt} &= \alpha_2 \frac{m_3^{n_2}}{K_{M2}^{n_2} + m_3^{n_2}} - m_2 \\
\frac{dm_1}{dt} &= \alpha_1 \frac{m_2^{n_1}}{K_{M1}^{n_1} + m_2^{n_1}} - m_1.
\end{aligned} \tag{1}$$

Later we will use this simplified model to illustrate control and dynamical systems theory methods to analyze its behavior. A more accurate, yet simple, model of the pathway is proposed in [29], including double phosphorylation steps for each kinase.

3 Analysis of Dynamic Behaviors

We can write the ODE model of a generic molecular process as:

$$\begin{aligned} \frac{dx}{dt} &= f(x,u), \\ x(0) &= x_0, \end{aligned} \tag{2}$$

where x is a vector in $\mathbb{R}^n$ whose components are the variables of interest in the model. In a system of molecules, these components are concentrations. Vector x describes the behavior in time of the system, and it is also called the state vector. Vector u in $\mathbb{R}^m$ represents external inputs to the system, for example concentrations of inducers or activating enzyme species. Function $f(x, u)$ captures the interactions among the chosen dynamic variables and the inputs. Finally, the problem includes a specification of initial conditions (or initial state) in the vector x_0.

Most models of biomolecular phenomena are nonlinear: thus, it is difficult (with few exceptions) to derive analytical predictions of their dynamics. The most general way to handle nonlinear systems is to analyze their dynamics in a neighborhood of their equilibrium points.

3.1 Linearization

Linearization analysis consists in approximating the behavior of a nonlinear system in a neighborhood of its equilibrium points using its linearized dynamics; a brief introduction to this technique is provided in this chapter, and the reader should refer to [30, 31] for more details.

The equilibrium points of the general dynamical system (Eq. 2) for a given value of external inputs $\overline{u}$ are defined as the states $\overline{x}$ such that $f(\overline{x}, \overline{u}) = 0$. In other words, if the system's state is precisely $\overline{x}$, all future states will remain equal to $\overline{x}$.

As a simple illustrative example, consider the differential equation:

$$\frac{dx}{dt} = ux - x^2 \tag{3}$$

If we set $\dot{x} = 0$, we find the condition $x(u - x) = 0$, which is satisfied for $\overline{x} = 0$, $\overline{x} = u$. Once the system's equilibrium has been found, we can write a Taylor series approximation for the system's dynamics near each equilibrium, stopping at the first order:

$$\begin{aligned} \frac{dx}{dt} = f(x,\overline{u}) &\approx \overbrace{f(\overline{x},\overline{u})}^{=0} + \left.\frac{\partial f(x,u)}{\partial x}\right|_{x=\overline{x},u=\overline{u}} (x-\overline{x}) \\ &\quad + \left.\frac{\partial f(x,u)}{\partial u}\right|_{x=\overline{x},u=\overline{u}} (u-\overline{u}) \\ &\approx J_x(x-\overline{x}) + J_u(u-\overline{u}), \end{aligned}$$

where J_x and J_u are constant scalars or matrices that capture the differential behavior of the system near the equilibrium. This procedure is the first step of linearization. Now with a change of variable, defining $\xi = (x - \overline{x})$ and $\omega = u - \overline{u}$ we can rewrite the system as:

$$\frac{d\xi}{dt} = J_x \xi + J_u \omega,$$

which is a linear dynamical system describing the near equilibrium dynamics of the original nonlinear system.

Going back to the illustrative example at Eq. 3, where $f(x, u) = ux - x^2$ we find that $J_x = \overline{u} - 2\overline{x}$, and $J_u = \overline{x}$. Therefore, the approximated system's dynamics near each equilibrium point are:

$$\overline{x} = 0 \quad \Rightarrow \quad \frac{d\xi}{dt} = \overline{u}\xi, \quad \overline{x} = \overline{u} \quad \Rightarrow \quad \frac{d\xi}{dt} = -\overline{u}(\xi - \omega),$$

where ξ and ω are values of the state and the input near the equilibrium.

For models defined by several states and differential equations, linearization yields a linear system described by two matrices:

$$J_x = \begin{bmatrix} \frac{\partial f_1}{\partial x_1} & \frac{\partial f_1}{\partial x_2} & \cdots & \frac{\partial f_1}{\partial x_n} \\ \frac{\partial f_2}{\partial x_1} & \frac{\partial f_2}{\partial x_2} & \cdots & \frac{\partial f_2}{\partial x_n} \\ \vdots & \vdots & \ddots & \vdots \\ \frac{\partial f_n}{\partial x_1} & \frac{\partial f_n}{\partial x_2} & \cdots & \frac{\partial f_n}{\partial x_n} \end{bmatrix}_{|x=\overline{x}, u=\overline{u}}, \qquad J_u = \begin{bmatrix} \frac{\partial f_1}{\partial u_1} & \frac{\partial f_1}{\partial u_2} & \cdots & \frac{\partial f_1}{\partial u_m} \\ \frac{\partial f_2}{\partial u_1} & \frac{\partial f_2}{\partial u_2} & \cdots & \frac{\partial f_2}{\partial u_m} \\ \vdots & \vdots & \ddots & \vdots \\ \frac{\partial f_n}{\partial u_1} & \frac{\partial f_n}{\partial u_2} & \cdots & \frac{\partial f_n}{\partial u_m} \end{bmatrix}_{|x=\overline{x}, u=\overline{u}}.$$

Matrix J_x is known as the system's Jacobian matrix. If the system of ODEs has n equations (states), the Jacobian is always an $n \times n$ matrix; J_u is an $n \times m$ matrix, where m is the number of external inputs.

Once the system has been linearized, we can investigate its local behavior with standard linear analysis methods. In particular, by finding the eigenvalues of the Jacobian we can immediately establish if the equilibrium is stable or unstable. Eigenvalues λ and eigenvectors v of a matrix A are defined by the following relationship:

$$Av = \lambda v.$$

If A is viewed as a linear map, eigenvectors represent special directions in the domain of A which remain unaltered in the codomain, except for scalar transformations. The eigenvalues of a matrix A are the roots λ of the polynomial equation:

$$\det(A - \lambda Id) = 0,$$

where $I\,d$ is the identity matrix of appropriate dimension. It is well known [31, 32] that the fundamental solution of a matrix ODE system $\dot{x} = Ax + Bu$ is determined by the matrix exponential

$\Phi = e^{At}$. (The natural response of the system, when $u = 0$, is $x(t) = e^{At}x_0$). In most practical cases, a real or complex matrix A is similar to a diagonal matrix Δ whose elements on the diagonal are the eigenvalues of A: $A = P\,\Delta\,P^{-1}$, where P is a matrix of eigenvectors associated with the eigenvalues of A. This means that we can rewrite the fundamental solution matrix $\Phi = e^{At} = Pe^{\Delta t}P^{-1}$ (the matrix exponential of a diagonal matrix is simply a diagonal matrix whose elements are the corresponding exponentials). Thus, the behavior of a linear system is given by linear combinations of exponential functions, whose convergent or divergent behavior exclusively depends on the sign of the eigenvalues. By determining the eigenvalues, and most importantly their sign, we can classify the system as stable, when all eigenvalues have a negative sign; when at most one zero eigenvalue is present, the system is classified as marginally stable; when at least one eigenvalue is positive, the system is unstable.

Finding the eigenvalues of J_x at each equilibrium allows us to build an approximate map of how the system behaves. Returning to our simple scalar example at Eq. 3:

$$\overline{x} = 0 \quad \Rightarrow \quad J_x = \overline{u}, \quad \overline{x} = \overline{u} \quad \Rightarrow \quad J_x = -\overline{u}$$

Therefore, for nonzero $\overline{u}$, the system always has one stable and one unstable equilibrium.

3.1.1 Linearization Example: The MAPK Cascade

We can carry out a linearization analysis of the MAPK cascade model (Eq. 1), choosing $\alpha_i = 1$ and $K_{Mi} = 1$ for $i = 1, 2, 3$, and $n_3 = 1$, $n_2 = n_1 = 2$:

$$\begin{aligned}
\frac{dm_3}{dt} &= \frac{u}{1+u} - m_3 \\
\frac{dm_2}{dt} &= \frac{m_3^2}{1+m_3^2} - m_2 \\
\frac{dm_1}{dt} &= \frac{m_2^2}{1+m_2^2} - m_1.
\end{aligned}$$

First, we find the equilibria by setting each derivative to zero. It is very easy to find that there is a single equilibrium where $\overline{m_3} = u/(1+u)$, $\overline{m_2} = \overline{m_3}^2/(1+\overline{m_3}^2)$, and $\overline{m_1} = \overline{m_2}^2/(1+\overline{m_2}^2)$. The Jacobian of the system is:

$$J_x = \begin{bmatrix} -1 & 0 & 0 \\ \alpha & -1 & 0 \\ 0 & \beta & -1 \end{bmatrix}, \tag{4}$$

where $\alpha = \frac{2\overline{m_3}}{(1+\overline{m_3}^2)^2}$ and $\beta = \frac{2\overline{m_2}}{(1+\overline{m_2}^2)^2}$. The eigenvalues can be read directly on the diagonal of J_x, because it is a lower triangular matrix. We find $\lambda_1 = \lambda_2 = \lambda_3 = -1$. Therefore, this system is stable near its single equilibrium point. Given the structure of the Jacobian and of

the ODEs, the equilibrium is stable regardless of the choice of parameters made. Therefore, this simplified model of the cascade suggests that its stable dynamic behavior is robust with respect to uncertainty in the parameters. We will later see that if the cascade includes additional interactions among the kinases, which generate feedback loops, we will not be able to reach the same conclusion.

3.1.2 Phase Portraits

Phase portraits are extremely useful graphical representations, in particular for models of low dimensions. The solution trajectories are parameterized over time, and plotted contrasting different components [31]. These graphs can be quickly traced qualitatively, and numerous numerical routines are available for quantitative plots (see, for example, MATLAB's `pplane` function).

For illustrative purposes, one typically considers second order linear systems, such as:

$$\begin{bmatrix} \frac{dx}{dt} \\ \frac{dy}{dt} \end{bmatrix} = A \begin{bmatrix} x \\ y \end{bmatrix}.$$

The system's phase portrait simply consists in a plot where $x(t)$ is graphed versus $y(t)$ on a plane. This plot can be quickly sketched by identifying the eigenvalues and eigenvectors of matrix A. The real part of the eigenvalues determines whether trajectories converge toward the origin as an equilibrium point (negative real part, equilibrium is stable) or diverge (positive real part, equilibrium is unstable); real eigenvectors define invariant subspaces on which the behavior of the trajectory is uniquely determined by the associated eigenvalue. Figure 1 shows typical examples of two-dimensional phase portraits, such as sinks (a), sources (b), and hyperbolic points (c). When eigenvalues are complex conjugates, trajectories spiral in or out of the origin depending on the sign of the real part (Fig. 1d,e); if the real part is zero, the system is classified as a center, i.e. a system whose trajectories oscillate without damping (Fig. 1f).

The only equilibrium of the MAPK pathway model considered in Subheading 3.1.1 is a sink (Fig. 1a), because all the eigenvalues of the Jacobian are real and have negative real part.

3.2 Bifurcations

If one or more parameters of the system vary, the number of equilibria and their local stability properties may change. In a biological network binding rates may vary as a function of environmental stimuli and result in dramatically different dynamic responses: for instance, there is evidence that MAPK pathway response can exhibit a variety of responses depending on the input hormones [33], which affect binding affinities of its components. The pathway is known to exhibit a multistationary (multiple equilibria either stable or unstable) or oscillatory responses [34]. The variation of one or more

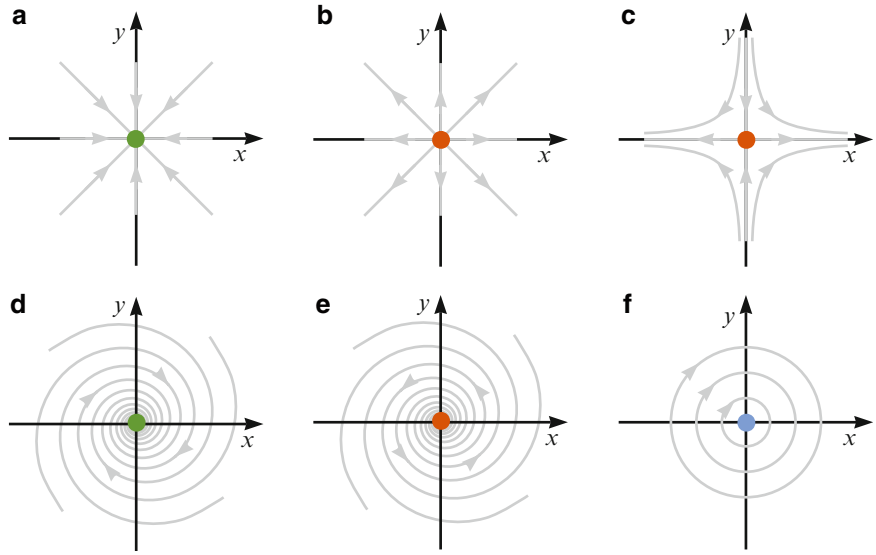

Fig. 1 Two-dimensional phase portraits. (**a**) Sink (all eigenvalues have negative real part). (**b**) Source (all eigenvalues have positive real part). (**c**) Hyperbolic point (one eigenvalue has positive real part, one eigenvalue has negative real part; eigenvectors coincide with the axes). (**d**) Stable spiral sink (eigenvalues are complex conjugate and have negative real part). (**e**) Unstable spiral sink (eigenvalues are complex conjugate and have positive real part). (**f**) Center (eigenvalues are pure imaginary, the system is marginally stable)

parameters followed by a change in dynamics is generally termed a bifurcation phenomenon. Classical examples are the saddle-node and the Hopf bifurcation [31]. Subheading 4.1 provides examples of bifurcations in a biological network with different types of feedback.

4 Feedback in Synthetic Biological Networks

Gene networks rely on feedback to regulate expression of proteins, reduce noise, and guarantee desired dynamic behaviors [35–38]. The target behavior of engineered networks depends as critically on the use of feedback: in this section we provide several examples of networks where the design of positive or negative feedback allows to achieve dramatically different behaviors. We begin with a general two-gene model which has been used to describe a variety of simple synthetic and natural networks; we show that in some cases the feedback topology is the key player in determining the dynamic outcomes of the system [7, 39]. Then, we highlight the effects of synthetic feedback loops on a model for the MAPK signaling pathway in yeast, which has recently been engineered to re-route mating behaviors [25].

4.1 Feedback Loops Reshape the Dynamic Behavior of a System

We consider a standard model for transcription and translation of two genes, where proteins reciprocally modulate their expression forming a feedback loop. Similar models are commonly encountered in the literature (see, for instance, [19, 22]). For illustrative purposes, we use a nondimensional model (*see* **Note 1**):

$$\dot{r}_1 = \gamma_1 + H_1(p_2) - r_1, \qquad \dot{p}_1 = \beta_1 r_1 - p_1, \tag{5a}$$

$$\dot{r}_2 = \gamma_2 + H_2(p_1) - r_2, \qquad \dot{p}_2 = \beta_2 r_2 - p_2, \tag{5b}$$

where, for $i = 1, 2$, r_i are RNA species concentrations; p_i are protein concentrations; $H_i(\cdot)$ are Hill functions, and all Greek letters denote reaction rates that are positive scalars.

Depending on the regulatory action and feedback created by the protein transcription factors, and thus depending on the type of Hill function, the network presents a different number of equilibria and different possible dynamic behaviors. For example, suppose $H_1(p_2) = \alpha_1 \frac{p_2^n}{1+p_2^n}$ and $H_2(p_1) = \alpha_2 \frac{p_1^n}{1+p_1^n}$: this is a two-gene positive feedback loop, which is often encountered in developmental networks [40, 41]. The Jacobian of the system is:

$$J = \begin{bmatrix} -1 & 0 & 0 & \frac{\partial H_1}{\partial p_2} \\ \beta_1 & -1 & 0 & 0 \\ 0 & \frac{\partial H_2}{\partial p_1} & -1 & 0 \\ 0 & 0 & \beta_2 & -1 \end{bmatrix}, \tag{6}$$

where $\partial H_i / \partial p_j = \alpha_i \frac{n p_j^{n-1}}{(1+p_j^n)^2}$, $(i, j) \in \{(1,2),(2,1)\}$. Note that the Jacobian entries, evaluated at a positive equilibrium, are sign definite, i.e. they do not change sign for arbitrary choices of the (positive) parameters α_i, β_i, and n.

The Jacobian sign pattern is thus a "structural" property of this system, and it can be associated with a graph: nodes correspond to the concentrations of biochemical species and are interconnected by positive $(+1)$ or negative (-1) arcs according to the corresponding Jacobian entries, as shown in Fig. 2a. Thus, the positive or negative sign of the loops generated does not depend on the specific choice of the parameters.

We can derive expressions for the equilibria of the system, which are given by the intersections of the two equilibrium conditions (Fig. 2a, top row):

$$p_1 = \beta_1 \left(\gamma_1 + \alpha_1 \frac{p_2^n}{1 + p_2^n} \right), \quad p_2 = \beta_2 \left(\gamma_2 + \alpha_2 \frac{p_1^n}{1 + p_1^n} \right).$$

For $n = 1$ there is an intersection with p_1 and p_2 positive. For $n > 1$, the system may admit multiple, typically three, positive equilibria. For an assigned value of n, we consider one equilibrium and we evaluate its stability properties by finding the eigenvalues of the Jacobian, which are the roots of its characteristic polynomial

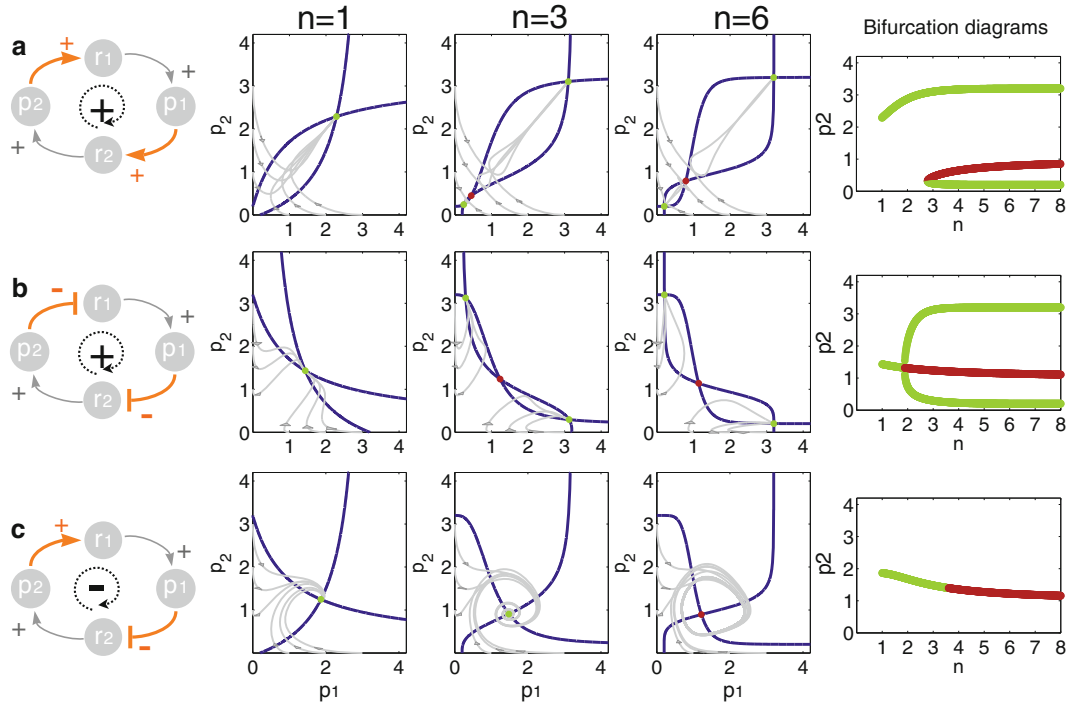

Fig. 2 Feedback loops in two-gene systems. (**a**) Two-gene system with double positive feedback loop (positive cycle). *Pointed arrowheads* indicate positive Jacobian interconnection entries, while *hammer-arrowheads* indicate negative interconnections. (**b**) Two-gene system with double negative feedback loop, resulting in an overall positive cycle. (**c**) Two-gene feedback interconnection with positive and negative regulation, resulting in an overall negative cycle. In all simulations (nullclines in *blue*, sample trajectories in *gray*) the nondimensional parameters are chosen as $\gamma_1 = \gamma_2 = 0.2$, $\alpha_1 = \alpha_2 = 3$, $\beta_1 = \beta_2 = 1$ and n is varied. The *right column* shows the corresponding value of p_2 equilibria for varying n, and their different pattern of transition to instability (*green dots* are stable, *red dots* are unstable equilibria)

$$(s+1)^4 - K = 0, \quad \text{where} \quad K = \beta_1\beta_2 \frac{\partial H_1}{\partial p_2}\frac{\partial H_2}{\partial p_1} > 0. \qquad (7)$$

Note that K explicitly depends on parameters n, α_i, and β_i and on the equilibria for p_1 and p_2 (which are in turn a function of all the parameters of the ODEs). The roots of Eq. 7 are:

$$s = -1 + q,\ -1 - q,\ -1 + iq,\ -1 - iq, \quad \text{where} \quad q = K^{\frac{1}{4}}.$$

If $K > 1$, there is only one root having positive real part, and it is real. If $K < 1$, all of the roots have negative real part. Thus, the system can only admit real exponential instability, i.e. instability arising due to a real eigenvalue changing sign from negative to positive. Figure 2a, top row, shows equilibrium conditions and example trajectories in the $p_1 - p_2$ plane of the phase space for different values of n (stable equilibria are represented as green circles, unstable equilibria as red circles). The last column in Fig. 2 shows the evolution of the number and stability properties

of equilibria for p_2 as n varies (note that other parameters could have picked to study the presence of bifurcations).

If $H_1 = \alpha_1 \frac{1}{1+p_2^n}$, $H_2 = \alpha_2 \frac{1}{1+p_1^n}$, network (Eq. 5) specifies a two-gene double negative feedback loop, depicted in Fig. 2b, left. This circuit is also known as toggle switch, an example of which is the famous synthetic biological circuit by Gardner [15]; a natural example of a toggle switch is the Cdc2-Wee1 network considered, for instance, in [4]. We can repeat the same analysis performed for the two-gene double positive feedback loop, and get similar results in terms of admissible transitions to instability, which can be only real exponential, regardless of the considered equilibrium (Fig. 2b).

We now compare the previous two examples to the case when Hill functions have opposite regulatory roles, i.e. $H_1 = \alpha_1 \frac{p_2^n}{1+p_2^n}$ an $H_2 = \alpha_2 \frac{1}{1+p_1^n}$: the network can behave as a two-gene oscillator [22]. First, we observe that the Jacobian is still a sign definite matrix. However, the "interconnection" terms $\partial H_1/\partial p_2$ and $\partial H_2/\partial p_1$, the derivatives of the Hill functions, now have opposite signs, due to the different slopes of such functions, and thus generate an overall *negative* feedback loop (Fig. 2c). The equilibrium conditions are now

$$p_1 = \beta_1 \left(\gamma_1 + \alpha_1 \frac{p_2^n}{1+p_2^n} \right), \quad p_2 = \beta_2 \left(\gamma_2 + \alpha_2 \frac{1}{1+p_1^n} \right),$$

and admit a single intersection regardless of the value of α_i, β_i, and n (Fig. 2c, central panels show the equilibrium conditions for increasing values of n). The characteristic polynomial is

$$(s+1)^4 - K = 0, \quad \text{where} \quad K = \beta_1 \beta_2 \frac{\partial H_1}{\partial p_2} \frac{\partial H_2}{\partial p_1} < 0. \tag{8}$$

Since now $K < 0$, all of the roots of Eq. 8 are complex:

$$s = (-1+q) + iq, \ (-1-q) - iq, \ (-1-q) + iq, \ (-1+q) - iq,$$
$$\text{where} \quad q = \frac{(-K)^{\frac{1}{4}}}{\sqrt{2}}.$$

As a consequence, only oscillatory unstable dynamics can arise, rather than real exponential. Precisely, unstable oscillations do arise when $K < -4$. As we can see by studying the original nonlinear system, for any given value of n there is only one equilibrium, whose stability properties can change, again, depending on the values of α_i and β_i.

To summarize, the analysis of this simple two-gene system has shown that, without a precise knowledge of the functions H_1 and H_2, we can reach very strong conclusions regarding the possible dynamic behaviors of the system. These conclusions are consistent with Thomas' conjectures [7], and do not depend on specific

functions or parameter choices. Rather, they depend on the presence of positive or negative feedback interconnection among components, thus on the presence of a positive or a negative cycle in the Jacobian associated with the system. In particular, this example clearly highlights that there is a relationship between Jacobian cycles and admissible transitions to instability. A qualitatively similar study was carried out and validated by building synthetic bacterial circuits in [16]; analysis relied on the S-systems formalism [42].

4.2 Synthetic Feedback in the MAPK Pathway

The dynamic profile of gene expression coordinates spatio-temporal processes in organisms. At the single-cell level, dynamics of signaling components can dictate the dynamics of gene expression and control cellular entry into divergent cell fates. The MAPK pathway in PC-12 cells provides a classic example of signaling dynamics regulating cellular fate. In PC-12 cells, unique extracellular cues alter the MAPK network topology by inducing positive or negative feedback loops leading to differential temporal profiles of MAPK activation. Each temporal profile maps to a distinct and divergent cellular behavior [33]. Synthetic switching of these topologies alters the dynamic profile and routes cells to the alternative fate, suggesting that control of network topology and thus signaling dynamics controls cellular fates (e.g., differentiation, division, and apoptosis). Given the importance of cellular fate in fields such as stem cell biology and cancer biology, synthetic circuits that can control dynamic signaling and thus cell fate may provide useful research tools as well as potential therapies.

Synthetic reshaping of dynamic signaling profiles in a MAPK pathway has allowed the construction of pulse generators, accelerators, delays, ultrasensitive responses, and bistable switches [43, 44]. Construction of positive feedback loops that induce bistability in a MAPK pathway was shown to be dependent on feedback strength [44]. Additionally, components within the MAPK pathway can be tuned to allow for the existence of bistability [45].

The yeast pheromone-responsive pathway is a canonical MAPK pathway with a three-tiered MAPK cascade. Due to the genetic tractability of yeast relative to mammalian systems, the pheromone-responsive pathway, also called the mating pathway, has been extensively analyzed experimentally and modeled computationally. Signaling in the mating pathway is initiated by pheromone alpha-factor (α), binding to a transmembrane receptor which initiates G-protein signaling and a phosphorylation cascade from Ste4 to the canonical scaffold-bound three-tiered MAPK cascade. As the output of the cascade, the phosphorylated MAPK Fus3 translocates the nucleus, activating transcription factors and transcription at mating-responsive genes including the *Fus1* locus. The phosphatase Msg5 antagonizes (inhibits) signaling by dephosphorylating Fus3. Activation of mating genes induces cell-cycle arrest, polarized

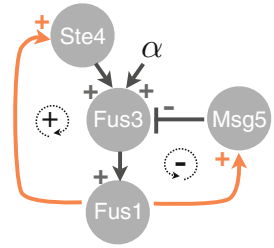

Fig. 3 Scheme of the engineered MAPK pathway in Eqs. 9–12. This scheme can also be seen as a graph representing the sign-definite Jacobian. *Orange arrows* indicate the synthetic feedback loops

cell growth, and fusion of haploid cells to form diploids with opposite mating-type cells.

To synthetically rewire the topology of the mating pathway, positive and negative feedback loops were constructed around the native pathway in [25]. To construct feedback loops (Fig. 3), a pathway-responsive promoter was cloned from the *Fus*1 locus into plasmids. Ste4 overexpression was shown to initiate pathway activation, positively regulating pathway activity. Thus, a positive feedback loop was constructed by placing Ste4 under the regulation of the *Fus*1 promoter. Conversely, overexpression of Msg5 attenuated signaling, negatively regulating pathway activation. Pairing Msg5 with the *Fus*1 promoter constructed a negative feedback loop. Pairing positive and negative feedback constructs with RNA-based transducers of varying activity generated constructs with a range of feedback strengths. Experimentally, the strength of positive feedback was shown to dictate the pathway sensitivity to activation. Similarly, the strength of negative feedback correlated with the degree of pathway attenuation.

To mathematically capture insights into the synthetically wired system, a phenomenogical model of the MAPK pathway with synthetic feedback was also constructed [25]:

$$\frac{dSte4}{dt} = \beta_{Ste4} - \delta_{Ste4} Ste4 + \boxed{k_{pf} \frac{Fus1^{n_{pf}}}{K_{M,Fus1,pf}^{n_{pf}} + Fus1^{n_{pf}}}}, \tag{9}$$

$$\frac{dFus3}{dt} = \beta_{Fus3} - \delta_{Fus3} Fus3 + k_{\alpha} \frac{\alpha^n}{K_{M,\alpha}^n + \alpha^n} + k_{Ste4} \frac{Ste4^m}{K_{M,Ste4}^m + Ste4^m} - k_{Msg5} Fus3 \frac{Msg5^q}{K_{M,Msg5}^q + Msg5^q}, \tag{10}$$

$$\frac{dFus1}{dt} = \beta_{Fus1} - \delta_{Fus1} Fus1 + k_{Fus3} \frac{Fus3^p}{K_{M,Fus3}^p + Fus3^p}, \tag{11}$$

$$\frac{dMsg5}{dt} = \beta_{Msg5} - \delta_{Msg5} Msg5 + \boxed{k_{nf} \frac{Fus1^{n_{nf}}}{K_{M,Fus1,nf}^{n_{nf}} + Fus1^{n_{nf}}}}. \tag{12}$$

Terms corresponding to the engineered positive and negative feedback loops are highlighted inside boxes. It is an easy exercise to compute the system's Jacobian matrix; this matrix is sign definite, meaning that the sign of each entry does not depend on the parameters chosen. Because of sign definiteness, the scheme in Fig. 3 can be also used as a "graph" representation of the Jacobian matrix similar to those obtained in Fig. 2.

In the rest of this section we consider the cases where the system is added exclusively one feedback loop, positive in the first case (activation of Ste4 by Fus1), negative in the second (activation of Msg5 by Fus1). With numerical simulations we will highlight the potential for bistability of the system with positive feedback, and of oscillations in the system with negative feedback. Unless otherwise noted, we use the same parameters used in [25], which were fitted to experimental data (*see* Fig. 6).

4.2.1 A Synthetic Positive Feedback Loop Can Yield Bistability

If we add exclusively a positive feedback loop to the system, Msg5 can be seen as an input (possibly constant or slowly varying) to the main pathway (a scheme is in Fig. 4a). In the following, we indicate the Msg5 input as u. We also assume that the inducer α is absent. Thus, our equations reduce to:

$$\frac{dSte4}{dt} = \beta_{Ste4} - \delta_{Ste4} Ste4 + \boxed{k_{pf} \frac{Fus1^{n_{pf}}}{K_{M,Fus1,pf}^{n_{pf}} + Fus1^{n_{pf}}}}, \tag{13}$$

$$\frac{dFus3}{dt} = \beta_{Fus3} - \delta_{Fus3} Fus3 + k_{Ste4} \frac{Ste4^m}{K_{M,Ste4}^m + Ste4^m} - k_u Fus3 \frac{u^q}{K_{M,u}^q + u^q}, \tag{14}$$

$$\frac{dFus1}{dt} = \beta_{Fus1} - \delta_{Fus1} Fus1 + k_{Fus3} \frac{Fus3^p}{K_{M,Fus3}^p + Fus3^p}, \tag{15}$$

where again we highlight with a box the term introducing positive feedback in the network. In the absence of α factor, the network output self-activates to a high value due to the presence of feedback. This behavior is showed in the numerical simulations in Fig. 4: increasing values of rate k_{pf} results in stronger self-activation of the pathway.

To explore the potential for bistability, as done in the previous section we can find equilibrium conditions for *Ste4* and *Fus1*:

$$\overline{Ste4} = \frac{1}{\delta_{Ste4}} \left\{ \beta_{Ste4} k_{pf} \frac{\overline{Fus1}^{n_{pf}}}{K_{M,Fus1,pf}^{n_{pf}} + \overline{Fus1}^{n_{pf}}} \right\} \tag{16}$$

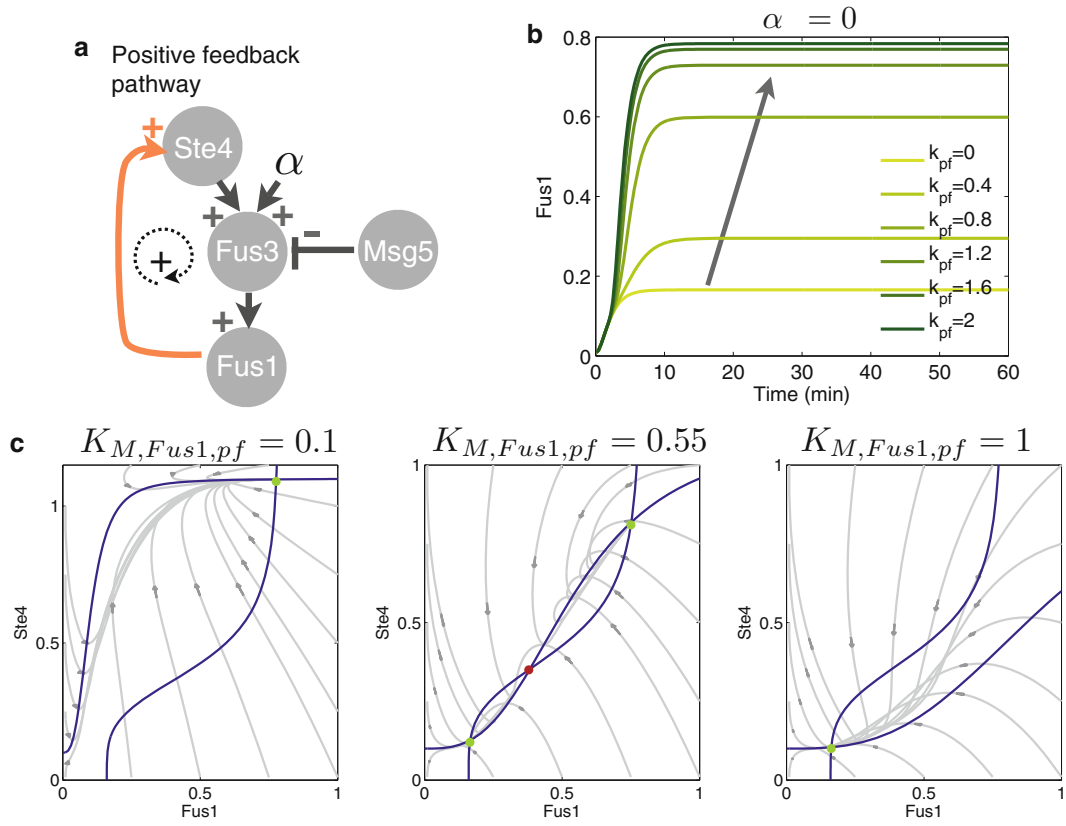

Fig. 4 Positive feedback pathway analysis. (**a**) Scheme of the network with positive feedback. (**b**) Concentration of Fus1 as a function of time, for different values of k_{pf}. (**c**) Equilibrium conditions (*blue*), their intersections (*green*, stable points; *red*, unstable points), and sample trajectories (*gray*) in the plane Fus1-Ste4. Bistability can be achieved when $K_{M,\,Fus1,\,pf}$ has values around 0. 5–0. 7

$$\overline{Fus3} = \frac{1}{\delta_{Fus3} + k_u \frac{u^q}{K_{M,u}^q + u^q}} \left\{ \beta_{Fus3} + k_{Ste4} \frac{\overline{Ste4}^m}{K_{M,Ste4}^m + \overline{Ste4}^m} \right\} \tag{17}$$

$$\overline{Fus1} = \frac{1}{\delta_{Fus1}} \left\{ \beta_{Fus1} + k_{Fus3} \frac{\overline{Fus3}^p}{K_{M,Fus3}^p + \overline{Fus3}^p} \right\}. \tag{18}$$

These equilibrium conditions depend on several parameters, each affecting the number and stability properties of the admissible equilibria. We focus our attention on the engineered reactions creating the positive feedback loop. We find that parameter $K_{M,\,Fus1,\,pf}$ is particularly important to achieve bistability; this parameter represents the half-max activation value of Ste4 by Fus1. The corresponding Hill coefficient is equal to 3, making the half-max value act as an activation threshold for Ste4. Equilibrium conditions Eqs. 16 and 18 are plotted in Fig. 4 for different values of $K_{M,\,Fus1,\,pf}(k_{pf} = 2)$. For the chosen parameter set, bistability is achieved only within a range of values of $K_{M,\,Fus1,\,pf}$:

4.2.2 A Synthetic Negative Feedback Loop Has the Potential to Yield Oscillations

We now numerically simulate the pathway in the presence of an engineered negative feedback loop only. In this case, Ste4 can be considered an external input, which we now call w. We assume that α factor is present. The ODEs are:

$$\frac{dFus3}{dt} = \beta_{Fus3} - \delta_{Fus3} Fus3 + k_\alpha \frac{\alpha^n}{K_{M,\alpha}^n + \alpha^n} + k_w \frac{w^m}{K_{M,w}^m + w^m} - k_{Msg5} Fus3 \frac{Msg5^q}{K_{M,Msg5}^q + Msg5^q}, \tag{19}$$

$$\frac{dFus1}{dt} = \beta_{Fus1} - \delta_{Fus1} Fus1 + k_{Fus3} \frac{Fus3^p}{K_{M,Fus3}^p + Fus3^p}, \tag{20}$$

$$\frac{dMsg5}{dt} = \beta_{Msg5} - \delta_{Msg5} Msg5 + \boxed{k_{nf} \frac{Fus1^{n_{nf}}}{K_{M,Fus1,nf}^{n_{nf}} + Fus1^{n_{nf}}}}. \tag{21}$$

The box highlights the negative feedback term; Fig. 5a shows the topology of this pathway, which corresponds to the sign pattern

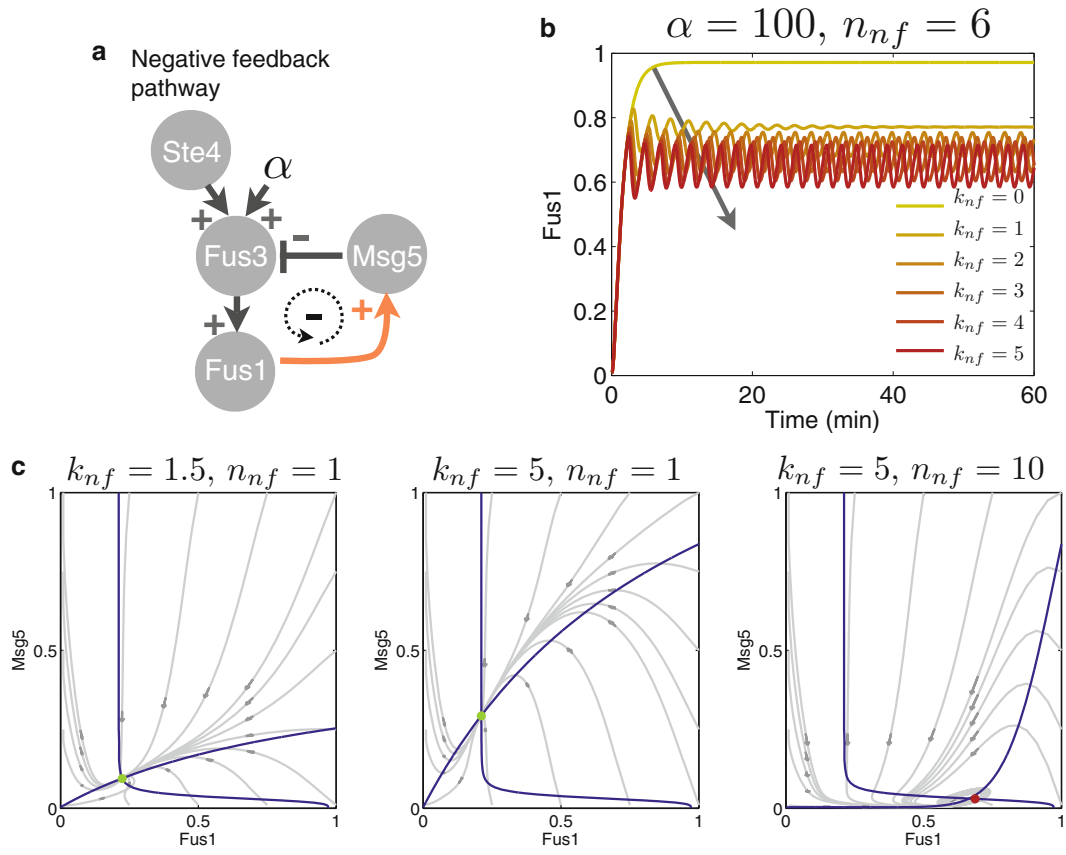

Fig. 5 Negative feedback pathway analysis. (**a**) Scheme of the network with engineered negative feedback. (**b**) Concentration of Fus3 as a function of time, for different values of k_{nf}. (**c**) Equilibrium conditions (*blue*), their intersections (*green*, stable points; *red*, unstable points), and sample trajectories (*gray*) in the plane Fus1-Msg5. Local oscillations can be achieved for high values of k_{nf} and n_{nf}. (Color figure online)

of the Jacobian matrix. Equilibrium conditions can be derived as done for the positive feedback pathway at Eqs. 16–18. To explore the potential for oscillations in the presence of negative feedback, we focus again on the parameters of the engineered reaction controlling Msg5 as a function of the output Fus1. Equilibrium conditions always intersect at one individual point, as shown in Fig. 5c. We find that for increasing values of both the rate k_{nf} and the Hill coefficient n_{nf}, the single equilibrium becomes unstable, with complex conjugate eigenvalues which correspond to local oscillations. The behavior in time of the output Fus1 is shown in Fig. 5b for a range of values of k_{nf}, and high $n_{nf} = 6$. For the chosen parameter set, our numerical analysis reveals that an extremely high value of k_{nf} and n_{nf} (experimentally not achievable) has the potential to yield oscillations, however their amplitude is limited and their frequency is very high. This means that experimentally it would be difficult to achieve oscillations in this particular synthetic pathway. More systematic exploration of the system's parameter space may reveal the existence of operating conditions that can yield more realistic oscillations.

5 Conclusions

In this chapter we have provided a general overview of the role of feedback in molecular networks. We have introduced simple yet powerful methods commonly used in dynamical systems and control theory to identify the behavior of a nonlinear dynamical system around its equilibria. Feedback loops dramatically affect the possible dynamic outcomes of a system: we showed that in some cases such outcomes may be determined exclusively by the type of feedback (positive or negative) present in the network, regardless of the parameters. We address the reader to [39] for further analysis on this topic. In some cases, parameters responsible for a bifurcation can be easily identified and tuned to achieve the desired behavior. These ideas have been largely exploited in the design of synthetic gene networks in the last decade [15, 16, 19, 20].

Throughout the chapter, we also used the MAPK pathway as an example of a system that can be successfully modeled with ODEs [5, 6, 25, 29] and lends itself well to the linearization analysis we presented. We focused on a recently engineered MAPK pathway in yeast, where positive and negative feedback loops were engineered using inducible promoters and RNA transducers [25]. Through numerical simulations, we showed that positive feedback can yield bistability and negative feedback can yield oscillations. We leave it as an exercise to the reader to verify the exclusive potential for bistability or oscillations in the two engineered versions of the network [39], following the steps outlined in Subheading 4.1 (Fig. 6).

Species	Description	β (production)	LB	UB
Fus1	Promoter activity, pathway output	0.001	1.00E-03	2
Fus3	MAPK, central hub in pathway	0.1	1.00E-03	1
Msg5	Native Msg5, negative regulator	0.01	1.00E-03	1
Ste4	Native Ste4, positive regulator	0.2	1.00E-04	0.5

Species	Description	δ (degadation)	LB	UB
Fus1	Promoter activity, pathway output	1	1.00E-03	3
Fus3	MAPK, central hub in pathway	0.7	1.00E-03	1
Msg5	Native Msg5, negative regulator	3	1.00E-03	5
Ste4	Native Ste4, positive regulator	2	1.00E-03	5

Rates	Description	Value	LB	UB
k_{α}	Rate constant for α-factor activation of Fus3	2	5.00E-01	4
k_{Fus3}	Rate constant for Fus3 activation of Fus1	1.3	1.00E-03	2
k_{Ste4}	Rate constant for Ste4 activation of Fus3	1	1.00E-03	5
k_{Msg5}	Rate constant for Msg5 desphosphorylation of	10	1.00E-03	15
$k_{c,Ste4}$	Rate constant for production of Ste4 from boo	2	1.00E-03	5
$k_{FB,Ste4}$	Rate constant for production of Ste4 from pos	2	1.00E-03	5
$k_{c,Msg5}$	Rate constant for production of Msg5 from res	2.5	1.00E-03	5
$k_{FB,Msg5}$	Rate constant for production of Msg5 from ne	1.5	1.00E-03	5

Hill coeff	Description	Value	LB	UB
n	Hill coefficient for α-factor effect on Fus3	2	1	5
n_{nf}	Hill coefficient for negative feedback loop, Fu	1	1	5
n_{pf}	Hill coefficient for positive feedback loop, Fus	3	1	5
m	Hill coefficient for Ste4 activation of Fus3	4	1	5
q	Hill coefficient for Msg5 deactivation of Fus3	4	1	5
p	Hill coefficient for Fus3 activation of Fus1	1	1	5

K_M	Description	Value	LB	UB
$K_{M,\alpha}$	Half-maximal concentration of α-factor (phero	14	10	40
$K_{M,Ste4}$	Half-maximal concentration of Ste4	0.5	1E-03	5
$K_{M,Msg5}$	Half-maximal concentration of Msg5	0.05	1E-03	5
$K_{M,Fus3}$	Half-maximal concentration of Fus3	1	1E-03	2
$K_{M,Fus1,nf}$	Half-maximal concentration of Fus1 for negati	1	1E-03	5
$K_{M,Fus1,pf}$	Half-maximal concentration of Fus1 for positiv	0.1	1E-03	5

Fig. 6 Parameters for the MAPK pathway model with *upper* (UB) and *lower* (LB) bounds for fitting

6 Notes

1. We will carry out the nondimensionalization procedure for the toggle switch network, leaving the derivation for the other cases to the reader. We follow nondimensionalization steps similar to those proposed in [19] and [22, 24]. Consider the (dimensional) model:

$$\tau \dot{R}_1 = c_1 + a_1 \frac{1}{K_{M1}^n + P_2^n} - R_1, \qquad \dot{P}_1 = k_p R_1 - k_d P_1, \quad (22a)$$

$$\tau \dot{R}_2 = c_2 + a_2 \frac{1}{K_{M2}^n + P_1^n} - R_2, \qquad \dot{P}_2 = k_p R_2 - k_d P_2. \quad (22b)$$

Here c_i is the "leak" transcription of RNA. For simplicity, we assume that the translation and degradation rates for the proteins are the same. Constant τ is the mRNA half-life in the system. Constants K_{Mi} represent the number of proteins necessary to half-maximally repress R_i. Finally, assume the translation efficiency of each RNA species is given by $\bar{p}_i$, which corresponds to the average number of proteins produced by a single RNA molecule.

We define the nondimensional variables: $r_i = R_i/\bar{p}_i$, $p_i = P_i/K_{Mj}$, $(i, j) \in \{(1, 2), (2, 1)\}$. We rescale time as $\tilde{t} = t/\tau$, and also define the nondimensional parameters:

$$\gamma_i = \frac{c_i}{\bar{p}_i}, \quad \alpha_i = \frac{a_i}{\bar{p}_i K_{Mi}^n}, \quad \beta_i = \frac{k_p \bar{p}_i}{k_d K_{Mj}}, \quad T = \frac{1}{\tau k_d}.$$

The resulting nondimensional equations are:

$$\dot{r}_1 = \gamma_1 + \alpha_1 \frac{1}{1 + p_2^n} - r_1, \qquad T\dot{p}_1 = \beta_1 r_1 - p_1, \quad (23a)$$

$$\dot{r}_2 = \gamma_2 + \alpha_2 \frac{1}{1 + p_1^n} - r_2, \qquad T\dot{p}_2 = \beta_2 r_2 - p_2, \quad (23b)$$

Finally, if we assume $T \approx 1$, we get a system in the same form as Eq. 5.

References

1. Tyson JJ, Chen KC, Novak B (2003) Sniffers, buzzers, toggles and blinkers: dynamics of regulatory and signaling pathways in the cell. Curr Opin Cell Biol 15(2):221–231
2. Hasty J, McMillen D, Collins JJ (2002) Engineered gene circuits. Nature 420:224–230
3. De Jong H (2002) Modeling and simulation of genetic regulatory systems: a literature review. J Comput Biol 9:67–103
4. Angeli D, Sontag E (2003) Monotone control systems. IEEE Trans Autom Control 48 (10):1684–1698
5. Huang C-YF, Ferrell JE (1996) Ultrasensitivity in the mitogen-activated protein kinase cascade. Proc Natl Acad Sci U S A 93:10078–10083
6. Asthagiri AR, Lauffenburger DA (2001) A computational study of feedback effects on signal dynamics in a mitogen-activated protein

kinase (MAPK) pathway model. Biotechnol Prog 17:227–239

7. Thomas R (1981) On the relation between the logical structure of systems and their ability to generate multiple steady states or sustained oscillations. In: Dora J, Demongeot J, Lacolle B (eds) Numerical methods in the study of critical phenomena. Springer series in synergetics, vol 9. Springer, Berlin/Heidelberg, pp 180–193
8. Domijan M, Pécou E (2011) The interaction graph structure of mass-action reaction networks. J Math Biol 51(8):1–28
9. Gouze J-L (1998) Positive and negative circuits in dynamical systems. J Biol Syst 6:11–15
10. Snoussi E (1998) Necessary conditions for multistationarity and stable periodicity. J Biol Syst 6:3–9
11. Banaji M, Craciun G (2009) Graph-theoretic approaches to injectivity and multiple equilibria in systems of interacting elements. Commun Math Sci 7(4):867–900
12. Kaufman M, Soule C, Thomas R (2007) A new necessary condition on interaction graphs for multistationarity. J Theor Biol 248 (4):675–685
13. Richard A, Comet J-P (2011) Stable periodicity and negative circuits in differential systems. J Math Biol 63(3):593–600
14. Soulé C (2004) Graphic requirements for multistationarity. ComPlexUs 1(3):123–133
15. Gardner TS, Cantor CR, Collins JJ (2000) Construction of a genetic toggle switch in *Escherichia coli*. Nature 403:339–342
16. Atkinson MR, Savageau M, Myers J, Ninfa A (2003) Development of genetic circuitry exhibiting toggle switch or oscillatory behavior in *Escherichia coli*. Cell 113:597–607
17. Kim J, White KS, Winfree E (2006) Construction of an in vitro bistable circuit from synthetic transcriptional switches. Mol Syst Biol 68
18. Padirac A, Fujii T, Rondelez Y (2012) Bottom-up construction of in vitro switchable memories. Proc Natl Acad Sci 109(47): E3212–E3220
19. Elowitz MB, Leibler S (2000) A synthetic oscillatory network of transcriptional regulators. Nature 403:335–338
20. Stricker J, Cookson S, Bennett MR, Mather WH, Tsimring LS, Hasty J (2008) A fast, robust and tunable synthetic gene oscillator. Nature 456:516–519
21. Tigges M, Marquez-Lago TT, Stelling J, Fussenegger M (2009) A tunable synthetic mammalian oscillator. Nature 457:309–312
22. Kim J, Winfree E (2011) Synthetic *in vitro* transcriptional oscillators. Mol Syst Biol 7:465
23. Montagne K, Plasson R, Sakai Y, Fujii T, Rondelez Y (2011) Programming an in vitro DNA oscillator using a molecular networking strategy. Mol Syst Biol 7
24. Franco E, Friedrichs E, Kim J, Jungmann R, Murray R, Winfree E, Simmel FC (2011) Timing molecular motion and production with a synthetic transcriptional clock. Proc. Natl Acad Sci 108(40):E784–E793
25. Galloway KE, Franco E, Smolke CD (2013) Dynamically reshaping signaling networks to program cell fate via genetic controllers. Science 341(6152):1235005
26. Tomita M, Hashimoto K, Takahashi K, Shimizu TS, Matsuzaki Y, Miyoshi F, Saito K, Tanida S, Yugi K, Venter JC, et al. (1999) E-CELL: software environment for whole-cell simulation. Bioinformatics 15(1):72–84
27. Hoops S, Sahle S, Gauges R, Lee C, Pahle J, Simus N, Singhal M, Xu L, Mendes P, Kummer U (2006) COPASINa complex pathway simulator. Bioinformatics 22(24):3067–3074
28. Kholodenko BN (2000) Negative feedback and ultrasensitivity can bring about oscillations in the mitogen-activated protein kinase cascades. Eur J Biochem 267(6):1583–1588
29. Angeli D, Ferrell JE, Sontag ED (2004) Detection of multistability, bifurcations, and hysteresis in a large class of biological positive-feedback systems. Proc Natl Acad Sci U S A 101(7):1822–1827
30. Khalil HK (2002) Nonlinear systems. Pearson Higher Education, Harlow
31. Perko L, (1991) Differential equations and dynamical systems. Springer, New York
32. Å strom KJ, Murray RM (2009) Feedback systems: an introduction for scientists and engineers. Princeton University Press, Princeton
33. Santos SDM, Verveer PJ, Bastiaens PIH (2007) Growth factor-induced MAPK network topology shapes Erk response determining PC-12 cell fate. Nat Cell Biol 9:324–330
34. Qiao L, Nachbar RB, Kevrekidis IG, Shvartsman SY (2007) Bistability and oscillations in the Huang-Ferrell model of MAPK signaling. PLoS Comput Biol 3(9):e184
35. Becskei A, Serrano L (2000) Engineering stability in gene networks by autoregulation. Nature 405(6786):590–593
36. Austin D, Allen M, McCollum J, Dar R, Wilgus J., Sayler G, Samatova N, Cox C, Simpson M (2006) Gene network shaping of inherent noise spectra. Nature 439(7076):608–611
37. Nevozhay D, Adams RM, Murphy KF, Josić K, Balázsi G (2009) Negative autoregulation linearizes the dose–response and suppresses the

heterogeneity of gene expression. Proc Natl Acad Sci 106(13):5123–5128

38. Rosenfeld N, Elowitz MB, Alon U (2002) Negative autoregulation speeds the response times of transcription networks. J Mol Biol 323:785–793
39. Blanchini F, Franco E, Giordano G (2013) A structural classification of candidate oscillators and multistationary systems. bioRxiv doi:10.1101/000562
40. Alon U (2006) An introduction to systems biology: design principles of biological circuits. Chapman & Hall/CRC, Boca Raton
41. Davidson EH, Rast JP, Oliveri P, Ransick A, Calestani C, et al. (2002) A genomic regulatory network for development. Science 295 (5560):1669–1678
42. Savageau MA, Voit EO (1987) Recasting nonlinear differential equations as s-systems: a canonical nonlinear form. Math Biosci 87:83–115
43. Bashor CJ, Helman NC, Yan S, Lim WA (2008) Using engineered scaffold interactions to reshape MAP kinase pathway signaling dynamics. Science 319(5869):1539–1543
44. Ingolia NT, Murray AW (2007) Positive-feedback loops as a flexible biological module. Curr Biol 17:668–677
45. O'Shaughnessy EC, Palani S, Collins JJ, Sarkar CA (2011) Tunable signal processing in synthetic MAP kinase cascade. Cell 144:119–131